This is the post print version of a Manuscript published in ACS Applied Materials and Interfaces at https://doi.org/10.1021/acsami.3c04206

Encapsulation of MCC950 in liposomes decorated with anti-Frizzled 1 improves drug bioavailability and effectiveness in fatty liver disease

Roberto Negro[a,‡], Rita Mastrogiacomo[b,c,‡], Livianna Carrieri[a,‡], Federica Rizzi[c], Valentina Arrè[a], Gianluca Minervini[a,c,d], Elisabetta Fanizza[b,c,e], Giusy Bianco[a], Annamaria Panniello[c], Marinella Striccoli[c], Roberto Comparelli[c], Raffaele Armentano[f], Maria Lucia Curri[b,c,e], Gianluigi Giannelli[g], Nicoletta Depalo[b] and Maria Principia Scavo[a*]*

[a] Laboratory of Personalized Medicine, National Institute of Gastroenterology, IRCCS "S. de Bellis" Research Hospital, Via Turi 27, Castellana Grotte, 70013 Bari, Italy

[b] Chemistry Department, University of Bari Aldo Moro, Via Orabona 4, 70125, Bari, Italy

[c] Institute for Chemical-Physical Processes, Italian National Research Council (IPCF)-CNR SS Bari,Via Orabona 4, 70125 Bari, Italy

[d] Department of Electrical and Information Engineering, Polytechnic of Bari, Via E. Orabona 4, Bari, 70126, Italy

[e] National Interuniversity Consortium of Materials Science and Technology, INSTM, Bari Research Unit, Chemistry Department, University of Bari Aldo Moro, Via Orabona 4, 70125, Bari

[f] Department of Pathology, National Institute of Gastroenterology "S. de Bellis," Research Hospital, Bari, Italy

[g] Scientific Direction, National Institute of Gastroenterology, IRCCS "de Bellis," Via Turi 27 Castellana Grotte, Bari, Italy

‡ Roberto Negro, Rita Mastrogiacomo and Livianna Carrieria contributed equally to this paper

* Email: n.depalo@ba.ipcf.cnr.it; maria.scavo@irccsdebellis.it

KEYWORDS. liposomes, luminescent Carbon dots, MCC950, NLRP3 inflammasome, liver cells

ABSTRACT

Inflammasome activation plays a crucial role in the progression to more severe stages of the Non-alcoholic fatty liver disease (NAFLD) representing a promising therapeutic target. MCC950 is a small molecule acting as potent and specific inhibitor of the canonical and non-canonical activation of NLRP3 inflammasome, but the short plasmatic half-life limits its use. Herein, we report, for the first time, on the encapsulation of the MCC950 in polyethylene glycol (PEG)-liposomes (LPs) that are specifically functionalized with an antibody against Frizzled 1 (FZD1), a g-coupled protein involved in the WNT pathway and overexpressed on the inflammasome activated macrophages. MCC950, encapsulated into PEG-LPs formulations conjugated with an anti-FZD1 antibody, inhibits the NLRP3 inflammasome activation at concentration value 10-times lower than the free drug in THP-1 cells. Luminescent Carbon dots (CDs) have been also co-encapsulated with MCC950 in LPs to obtain optically traceable nanoformulations that have proved the enhanced ability of the targeted LPs to be internalized into THP-1 cells respect to their not targeted counterparts. Our results suggest that the MCC950 encapsulation into targeted LPs represents a valuable strategy to achieve a re-formulation of the NLRP3 inhibitor able to significantly curtail

the threshold of MCC950 doses for inhibiting inflammasome activation thus offering a new therapeutic approach.

INTRODUCTION

The inflammatory state represents the hallmark of the Non-Alcoholic Steato Hepatitis (NASH), leading to necrosis of liver cells. The inflammation can origin outside the liver, such as in adipose tissue or in the gut, as well as inside the hepatic tissue (innate immune responses, mitochondrial dysfunction, lipo-toxicity, cell death pathways and generally cellular stress).[1] Immune cells, like lymphocyte subclasses and macrophages recruited at the inflammatory/necrotic sites, release cytokines and growth factors, as transforming growth factor (TGF)-β1, that stimulates the proliferation and activation of specialized fibroblasts, which then assume the phenotype of myofibroblasts. These myofibroblasts, known as hepatic stellate cells, are deputed to secrete extracellular matrix components, including collagens, fibronectins, laminins. The chronic inflammation together with the deposition of fibrotic tissue induce a rearrangement of the whole liver architecture and lead the worsening of liver damage up to cirrhosis and hepatocellular carcinoma (HCC) onset.[2] This immunologic milieu is enriched of activated macrophages characterized by an over-expression of the Frizzled protein 1 (FZD1), a g-coupled protein involved in the WNT pathway.[3] Macrophages participate to activation of the inflammasome, a multi-protein complex, emerging and leading mediator of the interaction among host and inflammatory cells based on the activation of the NLRP3 (NLR Family Pyrin Domain Containing 3). The inflammasome, then, activates specific proteins, such as caspase-1 and gasdermin D, which not

only guarantee the maturation and release of pro-inflammatory cytokines, like the circulating interleukin (IL) IL-1β , that play a key role in suppressing the immune response, but also induce cell death in a programmed form of inflammatory cell death called pyroptosis, that further contributes to the propagation of the inflammation itself.[4] Thus, an uncontrolled inflammasome activation determines a change on its protective role against the loss of tissue homeostasis, leading to the development of autoimmune pathologies, immunosuppression, cancer and onset of metastases.[5] MCC950 is an orally bioavailable small molecule acting as potent inhibitor of the NLRP3 inflammasome that has been evaluated in a multitude of NLRP3-driven inflammatory diseases.[6] Characterized by a short plasmatic half-life and by the lack of target capability, the clinical use of MCC950 could benefit from encapsulation in nanocarriers for improving its bioavailability and consequently therapeutic efficacy and inducing selective accumulation in the specific sites of inflammation associated with the NLRP3 inflammasome..

In literature, deployment of nanosystems for the not-specific inhibition of activation of components upstream of the NLRP3 has been reported. For example, not-targeted nanoparticles (NPs), composed of diselenide-containing molecules with oxidation-responsive properties, have been explored for the delivery of the SW033291, an inhibitor of prostaglandin-degrading enzyme that hampers liver regeneration.[7] Another nanosystem recently proposed to secondary inhibiting the NLRP3i mediated inflammasome is based on lactoferrin-modified LPs, able to specifically bind LRP1, a member of the LDLR family, that is ubiquitously expressed in several tissues and cells, such as vascular smooth muscle cells (SMCs), hepatocytes, and neurons as well as in the activated colonic macrophages, where they can reduce the levels of inflammatory cytokines and ROS and specifically suppress the MAPK/NF-κB pathway, with the secondary suppression also, among the others, of the NLRP3 inflammasome pathway.[8] However, the importance of univocally

targeting NLRP3 pathway is underpinned by its dominant role in the NASH induced liver degeneration.

"The delivery of the MCC950 by means of nanocarriers has been reported by L. Shun at al., that have developed a theranostic nanosystems based on polymeric NPs, co-encapsulating the MCC950 and a molecular probe, and demonstrated their effectively released by the NPs into the colon, at colonic pH, with high therapeutic efficacy of the MCC950 against ulcerative colitis due to activation inhibiting of the NLRP3 inflammasome.[9] Furthermore, platelet-derived extracellular vesicles loaded with the MCC950 have been prepared by Q. Ma et al. to prove their ability to selectively bind multiple cell types associated with formation of atherosclerotic plaques.[10]

However, the development of MCC950 loaded nanocarriers with inhibition efficacy on the NLRP3 inflammasome in the liver has still not been reported."

Here, polyethylene glycol (PEG) stabilized liposomes (LPs), have been decorated with an anti-FZD1 antibody, and loaded with the NLRP3 inflammasome inhibitor MCC950. Among synthetic nanovectors, LPs are highly biocompatible, versatile delivery nanosystems that can embed both hydrophilic, lipophilic and amphiphilic compounds for different applications.[11, 12] LPs represent the first example of drug delivery nanosystem approved by the FDA in 1995, accessible in the market and applied to human patients (Doxil).[13] Two LPs-based vaccines have been approved in 2021 against COVID-19. Interestingly, LPs not only can be explored as delivery vectors for various bioactive molecular compounds, but also for many functional nanoparticles (NPs).[12, 14] Indeed, in this study, luminescent CDs have been also co-encapsulated in LPs to obtain luminescent nanoformulations for *in vitro* monitoring the LPs cell uptake. Carbon dots (CDs) are luminescent NPs possessing outstanding optical properties and excellent biocompatibility, and

consequently they offer unique opportunity for developing optically traceable formulations valuable for bioimaging.[15-17]

This study aims at evaluating the bioavailability and effectiveness of the use of novel PEG stabilized LPs, decorated with anti-FZD1 antibody and loaded with the MCC950, to develop formulations for the selective targeting of the macrophages that, when activated, are directly involved in the Non-alcoholic fatty liver disease (NAFLD) progression to NASH.

RESULTS

PEGylated LPs-based formulations: preparation and characterization

Three different samples of PEG stabilized LPs encapsulating MCC950 (MCC950/LPs), (MCC950/LP 1, MCC950/LP 2 and MCC950/LP 3) have been prepared at increasing initial drug concentrations (0.3, 0.5 and 1 mg/mL), to investigate the most suited experimental conditions aiming at optimizing drug loading process. As control, empty LPs have been prepared under the same experimental conditions (Figure 1). The two, not completely resolved, peaks characterizing the UV-Vis absorption spectrum of MCC950, centered at 276 nm and 283 nm, respectively, can be also detected in the spectrum of the MCC950/LP sample, thus confirming the presence of the NRLP3 inhibitor in the nanoformulations (Figure 1 A-C).

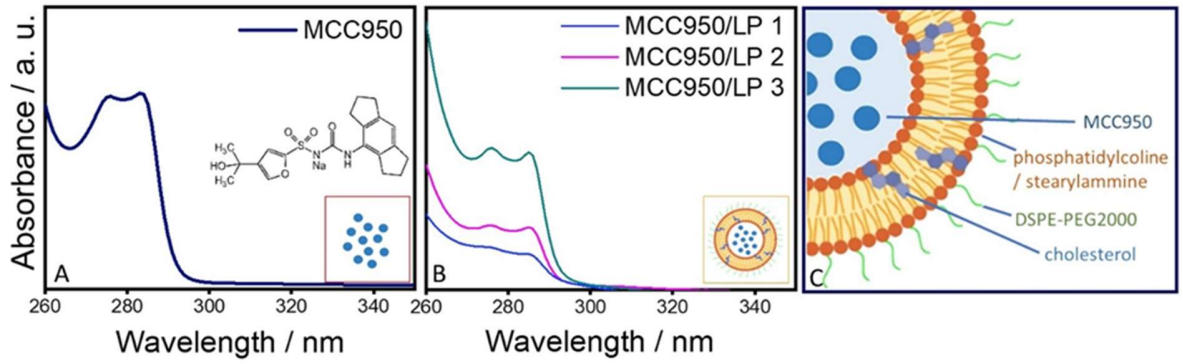

Figure 1. A) UV-Vis absorption spectrum and molecular structure of a MCC950 aqueous solution; B) UV-Vis absorption spectra of MCC950/LPs at different initial drug feeding; C) Schematic sketch of drug-loaded PEG-LPs. Drawings are not to scale.

Table 1. Table reporting the drug EE% and DL% values obtained for the different MCC/LPs samples.

Sample	[MCC950] (mg/mL)	EE (%)	DL (%)
MCC950/LP 1	0.3	93±5	1.6±0.2
MCC950/LP 2	0.5	58±3	2.4±0.2
MCC950/LP 3	1	60±3	7.5±0.4

A decrease in drug encapsulation efficiency percentage (EE%) and a corresponding increase in the drug loading percentage (DL%) have been achieved by increasing the MCC950 concentration from 0.3 up to 1 mg/mL (Table 1). Indeed, the maximum value of DL% has been obtained starting from 1 mg/mL of drug concentration (MCC950/LP3) that ends up with an actual MCC950 concentration of (0.20 ± 0.02) mg/mL in the resulting nanoformulations, which has been then used for the further developments and investigation.

The MCC950/LPs have been thoroughly characterized and compared to the empty LPs in terms of size, colloidal stability and morphology by means of DLS investigation, ζ-potential measurements and TEM analysis (Figure 2).

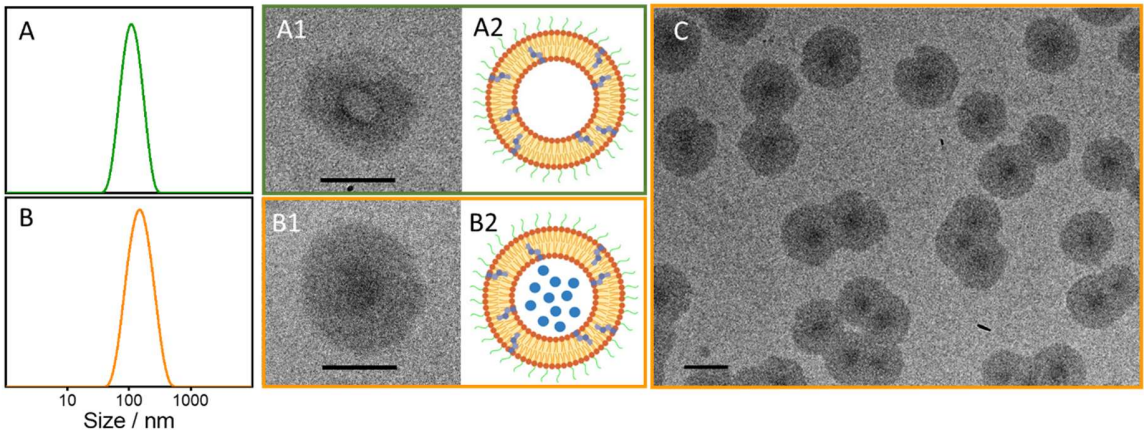

Figure 2. A-B) Representative size distribution by intensity, performed by DLS measurements, of empty LPs and MCC950/LPs; A1-A2; B1-B2) Close up of TEM micrograph (Scale bars 100 nm) along with the corresponding schematic sketches of empty LPs and MCC950/LPs; C) Large area TEM micrograph of MCC950/LPs (Scale bar 100 nm).

Table 2. Summary of size, PDI and ζ-potential values of empty LPs and MCC950/LPs.

Sample	Size (nm)	PDI	ζ-Potential (mV)
Empty LPs	102±2	0.175±0.011	20±3
MCC950/LPs	151±1	0.245±0.010	-22±2

The two investigated type of samples resulted, by DLS investigation, having a mean hydrodynamic diameter of (102 ± 2) and (151 ± 1) nm, respectively for empty LPs and MCC950/LPs (Figure 2 A, B and D) with a monomodal size distribution (Table 2). The TEM micrographs recorded for the empty or the MCC950 loaded LPs (Figure 2 A1, B1 and C) show in both cases rounded shape objects, with spherical morphology and size comparable to that resulting

from DLS analysis. Interestingly, the empty LPs present an external circular dark grey region, reasonably ascribable to the bilayer structure along with an internal light grey core, due to the inner domain (Figure 2 A1). Conversely, the MCC950/LPs sample shows the presence of a core even darker than the surrounding circular structure can be attributed to the presence of the hydrophilic drug in the inner aqueous compartment of the LPs (Figure 2 B1 and C). The ζ-potential measurements (Table 2) on the empty LPs result in positively charged surface, reasonably due to the charged amino group of the stearylamine, used for their preparation. The loading with MCC950, which is in form of sodium salt, shifts the ζ-potential towards negative value. ATR FT-IR analysis carried out on free drug, empty LPs and MCC959/LPs further confirms the actual drug load of the LP-based nanoformulations (Figure S1, SI).

To prepare luminescent LPs, firstly, oil-soluble CDs exhibiting tunable light emission properties in the visible spectrum have been synthesized[18] (Figure S2, SI), and two CDs loaded LPs samples, namely CD/LPs and MCC950-CD/LP, both at starting CD amount of 5 mg and at initial drug feeding of 1 mg/mL (Figure 3 and Figure S3, SI).

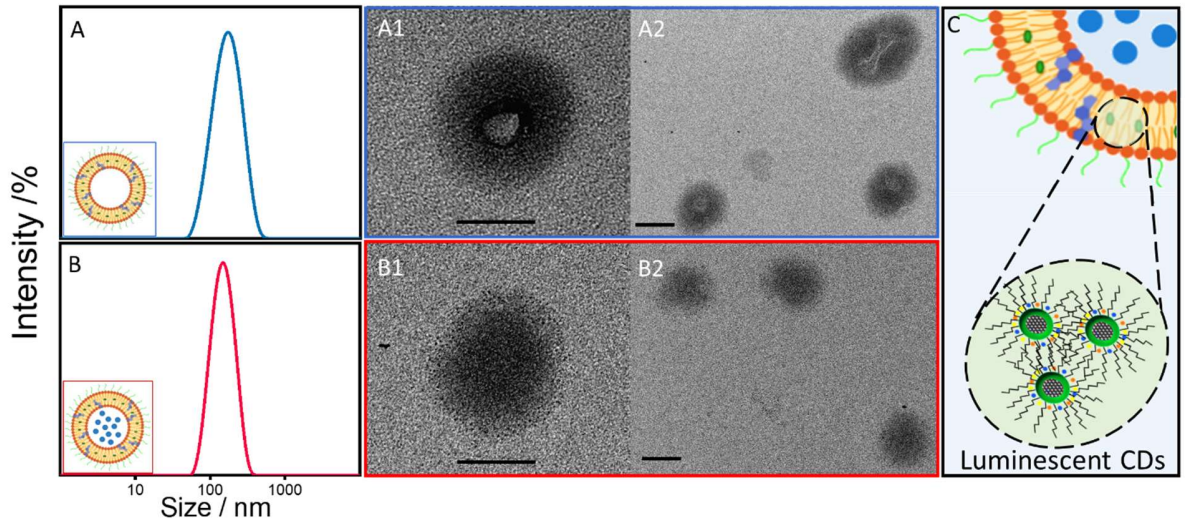

Figure 3. A-B) Representative size distribution by intensity, performed by DLS measurement of CD/LPs and MC950-CD/LPs; A1-A2; B1-B2) TEM micrograph and corresponding close up, along with their schematic sketch, of CD/LPs and MCC950-CD/LPs, respectively (Scale bar 100 nm); C) Schematic sketch of the MCC950-CD/LPs that highlights the CDs assembled in the LP bilayer. Drawings are not to scale.

Table 3. Summary of size, PDI and ζ-potential values of the CD/LPs and MCC950-CD/LPs.

Sample	[Drug Feeding] (mg/mL)	CD Feeding (mg)	Size (nm)	PDI	ζ-potential (mV)
CD/LP	-	5	161±2	0.217±0.012	35±2
MCC950-CD/LP	1	5	164±3	0.222±0.012	-16±2

DLS investigation performed on the CD/LPs and MCC950-CD/LPs samples indicated, for both samples, monomodal size distribution and mean hydrodynamic diameters of (161 ± 2) nm and (164 ± 3) nm respectively (Figure 3 A-B, Table 3). The TEM micrographs of the two samples (Figure 3 A1, A2, B1, B2, and Figure S3 B and B1, SI) reveal, in the round shaped objects, the presence of black spots having size comparable to those of the *as synthesized* CDs (Figure S2 A. In particular, in the case of the CD/LPs, it is possible to observe a dark grey region, reasonably ascribable to the bilayer encapsulating the hydrophobic CDs, while a uniform lighter grey area can be assigned to the hydrophilic core of the structure (Figure 3 A1 and A2). For the MCC950-CD/LPs, the inner aqueous domain, encapsulating the hydrophilic drug cannot be distinguished from the outer circular corona, assigned to the bilayer, as both regions appear dark grey (Figure 3 B1 and B2) thus suggesting the actual modification of the core composition. The ζ-potential analysis of CD/LPs and empty LPs points out a positively charged surface that reach negative values, when the MCC950 is added to the nanoformulations, and therefore indicating that MCC950 can be also partially adsorbed on the LPs surface (Table 3). The drug loading and the CDs encapsulation in the LPs have been further investigated by an advanced spectroscopic analysis.

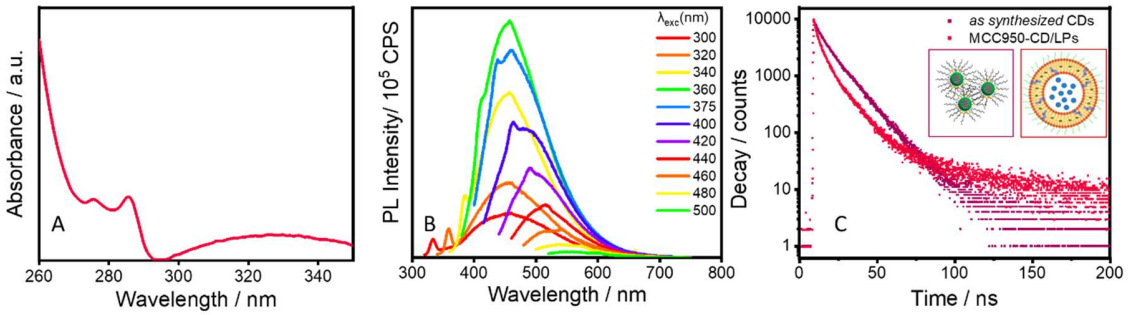

Figure 4. A) UV absorption spectrum of the MCC950-CD/LPs; B) Steady-state PL spectra of the MCC950-CD/LPs dispersed in water, recorded at various excitation wavelengths. C) TR-PL study measured at λ_{em} = 460 nm for λ_{exc} = 375 nm performed on *as synthesized* CDs and MCC950-CD/LPs dispersed in chloroform and water, respectively.

Table 4. Table reporting the drug EE% and DL% values obtained for MCC950-CD/LPs.

	MCC 950	
Sample	**EE%**	**DL%**
MCC950-CD/LP	53±3	20.0±1.5

The absorption spectrum of the MCC950-CD/LPs (Figure 4 A) demonstrates that both the drug and the CDs are present in the nanoformulations, as confirmed by the absorption signal at higher wavelength, characterized by the peculiar line profile of the drug (Figure 1 A), and by the one at lower wavelength (350 nm) that can be safely attributed to the CDs (Figure S2 C, SI).

The PL spectra the MCC950-CD/LPs dispersed in aqueous solution show the typical excitation wavelength-dependent fluorescence of CDs (Figure S2 D, SI) To note, this indicates that also encapsulated CDs retain their optical properties (Figure 4 B). The spectrum of this sample, when compared to *as synthesized* CDs, exhibit an additional narrow Raman peak at higher energy, that shifts at the increase of the excitation wavelength. Such peak can be ascribed to a Raman symmetric stretching of O-H bonds of water used, in this case, as solvent to disperse the sample.

To further investigate the nature of the luminescence recorded for the MCC950-CD/LPs, time-resolved photoluminescence (TR-PL) measurements have been performed on both the *as synthesized* CDs and the MCC950-CD/LPs samples. Both the decays have been best fitted by using a multiexponential model function and the average lifetimes (τ_{avg}) have been calculated, resulting of 8.9 ns for the pristine CDs and of 6.4 ns for MCC950-CD/LPs. Consequently, CDs embedded in LPs and dispersed in water are characterized by a shorter lifetime when compared to the pristine CDs, dispersed in chloroform, indicating the presence of non-radiative recombination channels ascribed to a possible modification of the chemical environment and dispersing medium with respect to free CDs in organic solution. Moreover, for the embedded CDs the decay does not goes to zero, probably due to residual LPs scattering. Absolute photoluminescence quantum yield (PLQY, Figure S2 D, SI) measured at 375 nm (λ_{exc} corresponding to the maximum of intensity in the CDs PL spectrum) has resulted (10 ± 5) %, that is lower than that found for the *as synthesized* CDs ((26.2 ± 0.5) %, SI). Such differences can be ascribed to the change in the environment of CDs once they are encapsulated into LPs, since CDs emission properties arise also from the CDs surface.[16] Therefore the spectrofluorometric investigation confirms the outcome of the TEM investigation, indicating that the CDs are embedded in LPs. Finally, the EE% and DL% values obtained for the MCC950 in LPs have been (53±3) and (20.0±1.5%), respectively (Table 4). The EE% of the CDs encapsulated in the MCC950-CD/LPs has been also evaluated by PL measurements (Figure S3, SI) resulting about 72% (Figure S3 C, SI).

Finally, the two LPs-based samples conjugated with the antiFZD1 antibody to obtain the anti-FZD1/MCC950/LPs and the luminescent anti-FZD1/MCC950-CD/LPs have been prepared and characterized (Figure 5). TEM analysis of the two targeted formulations (Figure 5 A-B) does not point out any significant change in their morphology when compared with their no conjugated

counterparts (Figure 2 B1 and C, Figure 3 B1 and B2). For both the conjugated samples, a slight decrease in DL% has been achieved, reasonably due to the various steps required for the conjugation (Table 5). The results of the DLS investigation and ζ-potential measurements for the two samples are consistent with the corresponding not targeted formulations (Table 5). FTIR-ATR spectroscopic analysis (Figure S4, SI) allows to qualitatively assess the presence of the antibody on the surface of the LPs.

The quantification of the anti-FZD1 antibody, indirectly performed by using a secondary fluorescent antibody as a labelling agent, has resulted in (6.0±0.7) μg/mL average concentration of anti-FZD1 conjugated to either the anti-FZD1/MCC950/LPs or anti-FZD1/MCC950-CD/LPs samples. (Figure S5, SI).

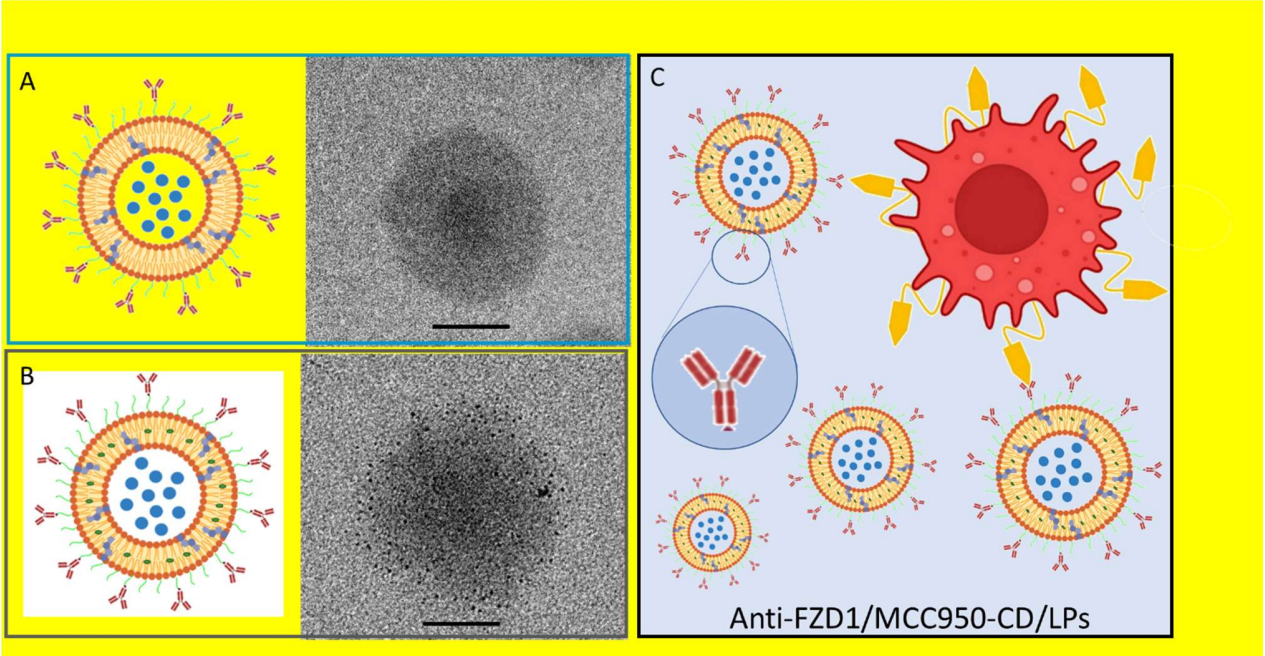

Figure 5. Close up of TEM micrographs along with the corresponding schematic sketch of the A) anti-FZD1/MCC950/LPs and B) of the anti-FZD1/MCC950-CD/LPs (Scale bar 100 nm); C) Schematic representation of molecular recognition between anti-FZD1/MCC950-CD/LPs and NLRP3 inflammasome activated THP-1 cells overexpressing the FZD1 molecular receptor. Drawings are not to scale.

Table 5. Summary of size, PDI and ζ-potential values recorded for the anti-FZD1/MCC950/LPs and anti-FZD1/MCC950-CD/LPs samples.

Sample	Size (nm)	PDI	ζ-potential (mV)	EE (%)	DL (%)
Anti-FZD1/MCC950/LPs	155±2	0.168±0.019	-22±2	55±4	6.9±0.4
Anti-FZD1/MCC950-CD/LPs	167±2	0.290±0.030	-28±2	50±2	18.0±0.3

Cell uptake of the LP-based formulations

THP-1 cells have been incubated with MCC950-CD/LPs and with anti-FZD1/MCC950-CD/LPs at the concentration of 1 nM for MCC950 and 0.0336 mg/mL for CD for 1, 4 and 8 hours, to monitor the cellular uptake of the LPs by means of confocal microscopy.

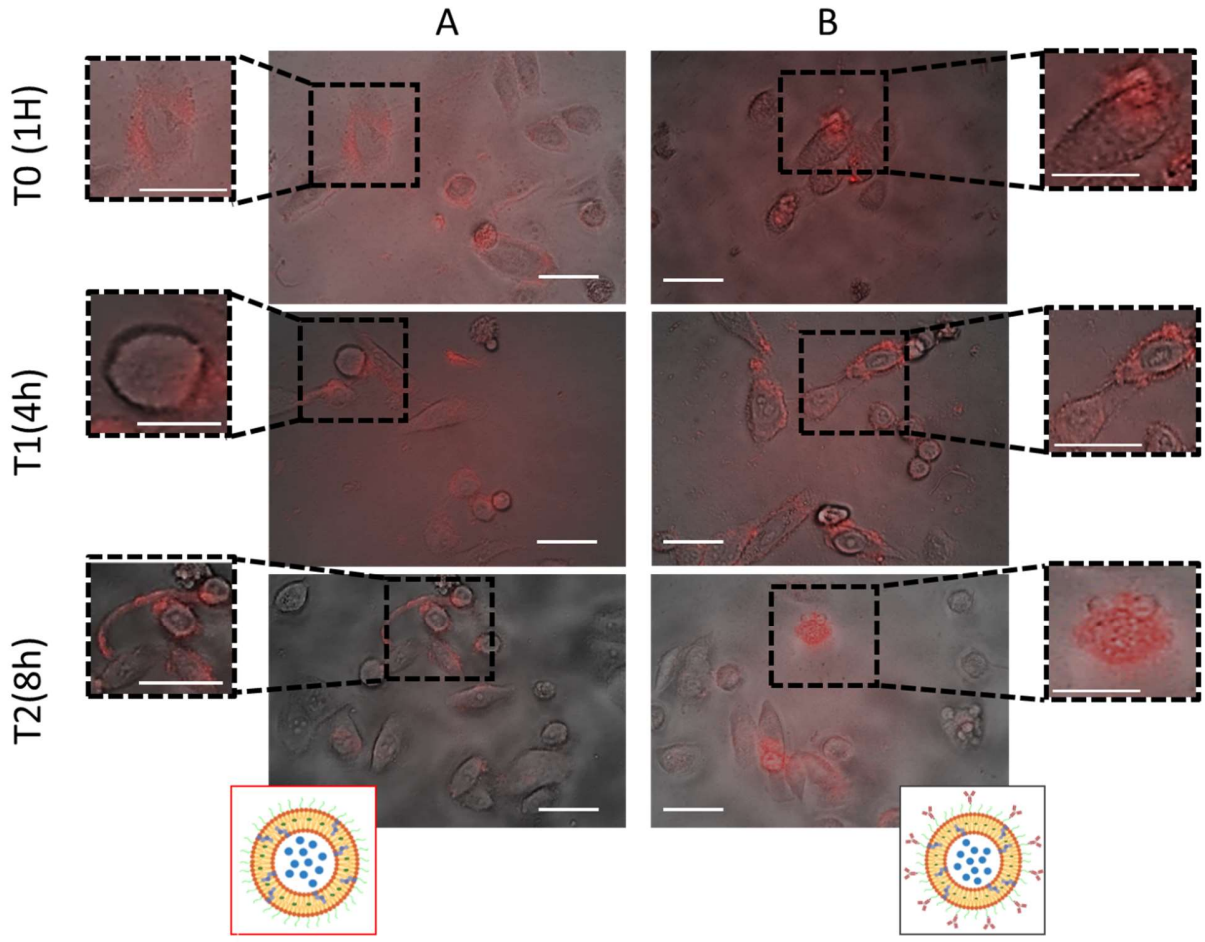

Figure 6. Representative confocal fluorescence micrographs of fixed THP-1 cells. Time-dependent uptake of the fluorescent MCC950-CD/LPs and anti-FZD1/MCC950-CD/LPs in THP-1 cells. Overlay of bright field and red channel of the cells treated with MCC950-CD/LPs (A) and anti-FZD1/MCC950-CD/LPs (B) for 1, 4 and 8 hours. Scale bar, 50 μm. λ_{ex}=555 nm. Magnification, 40×.

After 4 hours incubation with MCC950-CD/LPs, the fluorescent not targeted LPs have been localized outside of cells, while after 8 hours, they have been found still accumulated on cell membranes (Figure 6A). Under the same experimental conditions, after 1 hour the fluorescent targeted LPs have been observed outside the cells, while after 4 hours they found migrated in the

cytoplasm (Figure 6B). Finally, after 8 hours only the anti-FZD1/MCC950-CD/LPs, and not the not targeted counterpart, have been seen completely uptaken in the cells.

Cell viability of LP-based formulations

The effects of free MCC950 and of the drug encapsulated in LPs formulations (MCC950/LPs and the anti-FZD1/MCC950/LPs) on THP-1, HEPA-RG and HLF cell viability have been evaluated by means of MTS proliferation assay. In all the experiments, at 24, 48, and 72 hours, 1 nM MCC950 has been used, either administered as free or encapsulated in LPs. In addition, cells have been treated with empty LPs, as control, prepared at the same lipid concentration used for the drug loaded LPs. Upon the treatment, the viability of all cell lines has been found higher than 99% when incubated with empty LPs and with MCC950, either when administrated as free or encapsulated into LPs (Figure 7), thus indicating, under the investigated conditions, the absence of any cytotoxic effect of MCC950 nor free in the preparation or encapsulated in LPs formulations.

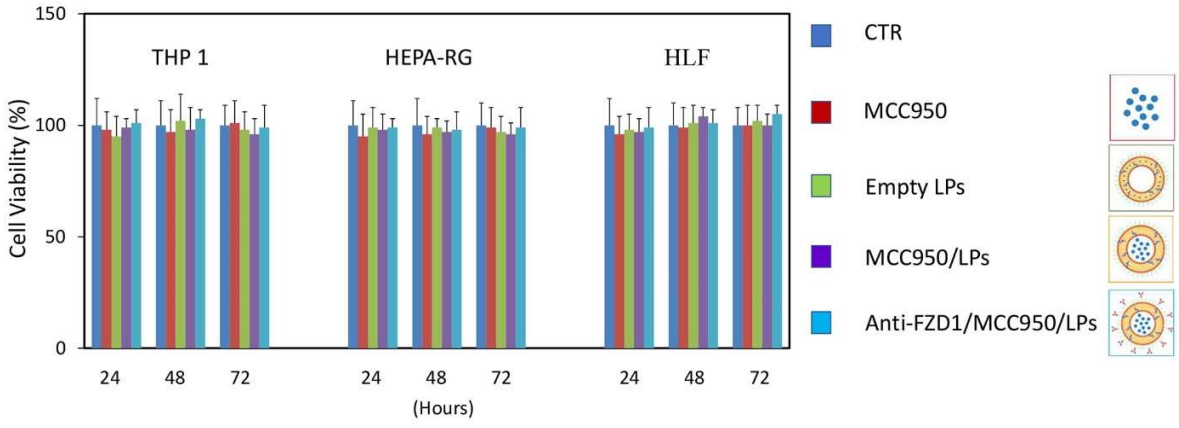

Figure 7. Viability results by MTS assay for THP-1, HEPA-RG and HLF cells after cell incubation for 24, 48 and 72 h with free MCC950, empty LPs, MCC950/LPs and

antiFZD1/MCC950/LPs. Control (CTR): Untreated cells. Data presented as mean ± standard error of three distinct experiments performed in triplicate.

To test the MCC950 effectiveness, the inflammasome has been activated by treating THP-1 cells with LPS/Nigericin and the resulting activation has been monitored by numbering the presence of ASC punctum, that are apoptosis-associated speckle-like protein containing a caspase activating and recruitment domain, by means of immunofluorescence (Figure 8A-B). Then, after the inflammasome activation by LPS/Nigericin (Figure 8 B2), THP-1 cells have been treated with MCC950 either free (Figure 8 B3) or encapsulated in the not targeted LPS, namely MCC950/LPs (Figure 8 B5) and antiFZD1/MCC950/LPs at 1 nM (Figure 8 B6). Free MCC950 has been found to partially reduces the number of puncta (detected as red spot) as much as the empty LPs can do (Figure 8 A, 8 B3 and 8 B4). On the contrary, the MCC950/LPs have demonstrated to reduce puncta much more than Lipopolysaccharide (LPS)/Nigericin and empty LPs; the anti-FZD1/MCC950/LPs treatment strongly reduce the number of puncta (Figure 8 A, 8 B5 and 8 B6). These data suggest that the MCC950 is able to inhibit inflammasome activation only to a limited extent when administered as free, whereas it blocks inflammasome activation when encapsulated in LP decorated with the anti-FZD1 antibody.

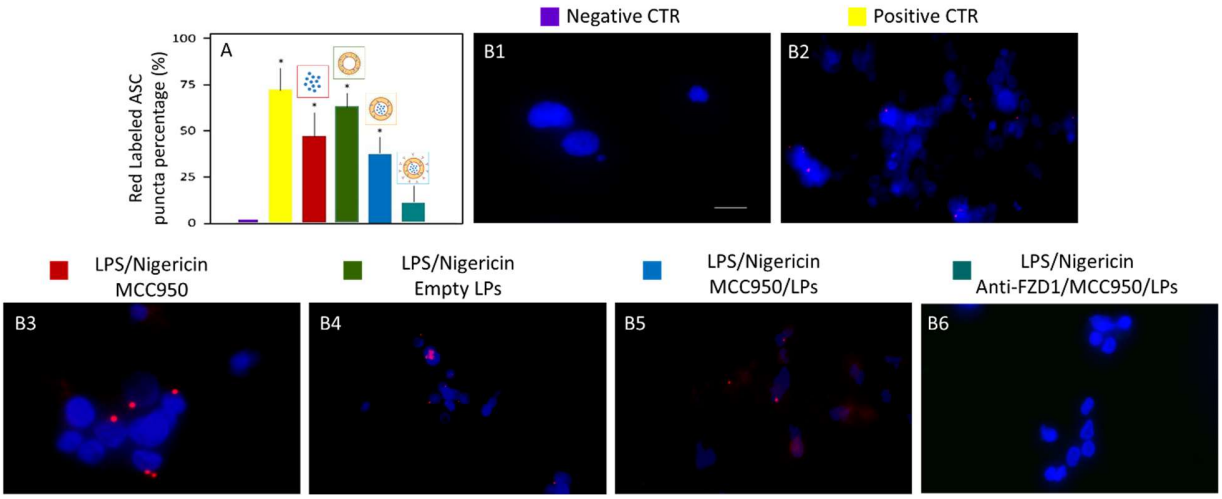

Figure 8. (A) Number of spots (as percentage) of ASC *puncta* in the THP-1 cells treated with LPS/Nigericin (positive control), LPS/Nigericin and MCC950, LPS/Nigericin and empty LPs, LPS/Nigericin and MCC959/LPs, and finally LPS/Nigericin and anti-FZD1/MCC959/LPs, expressed as percentage respect to untreated cells (CTR); (B) Detection of ASC *puncta* of inflammasome by immunofluorescence confocal microscopy in the fixed THP-1 cells. Overlay of blue stained nuclei and red labeled *puncta* of negative CRT (untreated cells, B1) and positive CRT (cells treated with LPS/nigericin, B2), LPS/Nigericin and MCC950 (B3), LPS/Nigericin and empty LPs (B4), LPS/Nigericin and MCC959/LPs (B5), and LPS /Nigericin and anti-FZD1/MCC959/LPs (B6). Scale bar, 50 μm. λ_{ex}=555 nm (red channel), λ_{ex}=358 nm (blue channel). Magnification, 40×.

Effectiveness of LP-based formulations on proinflammatory cytokine secretion

To investigate the down streaming inhibitory effect of MCC950 on inflammasome activation, the secretion of the pro-inflammatory cytokine, IL-1β, has been measured after 72 hours of treatment. Free MCC950 and empty LPs have been used as control.

IL-1β levels have been measured in the medium of inflammasome-activated THP-1 cells as well as of human hepatocytes and hepatocellular carcinoma cells (Figure 9). IL-1β levels have been found significantly higher (**$p<0.001$) for THP-1 upon LPS/Nigericin treatment (Positive control), as well as upon incubation with empty LPs (**$p<0.001$). A significantly drastic reduction

of IL-1β levels has been detected upon the anti-FZD1/MCC950/LP (1 nM of MCC950) treatment, that become comparable with the control. The increase of the IL-1β levels in comparison to the control cells has been also observed in the THP1 cells treated with the free MCC950. No significant variation of IL-1β level has been detected within the medium derived from HLF and HEPA-RG.

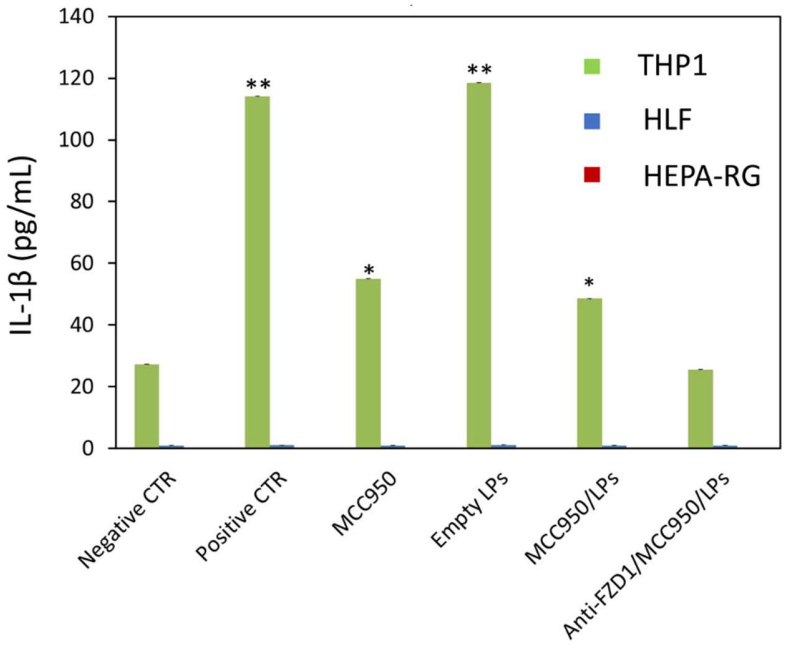

Figure 9. Quantitative analysis of IL-1β within the medium of inflammasome-activated THP-1 cells, IL-1β level within the medium of the three individual cell lines, referred to control cells. Control (CTR): Untreated cells (*p<0.005; ** p<0.001).

Therapeutic effectiveness of LPs-based formulations on *in vivo* fatty liver models

Finally, to test the hypothesis that encapsulating MCC950 in PEGylated LPs decorated with anti-FZD1 antibody improves the effectiveness of the drug used as free, we fed 12 wild type mice with a high fat diet for 1 month, and, under the same experimental conditions, the animals have been

treated with LPS/Nigericin to induce inflammasome. Furthermore, all animals also received Dextran-Sulphate-Sodium (DSS), that associated with a high-fat diet leads to liver inflammation.[19, 20] Mice have been randomly divided in four groups, namely wild type mice receiving only the high fat diet used as control group and three groups receiving free MCC950, MCC950/LPs or anti-FZD1/MCC950/LPs, respectively. One week after the end of the treatment the animals have been sacrified, then the liver has been explanted and processed for haematoxylin–eosin (He-E) and Gomori's reticulin staining (Figure 10). Liver sections of mice treated with targeted and not targeted LPs, free drug, or untreated (CTR), stained for He-E at 20x and 40x of magnification are reported in Figure 10 A. In the control group inflammation sites have been found developed around the portal space, with A2 coefficient of inflammation (Table 1). In mice treated with 1 mg/kg of free MCC950, the inflammation has been observed still present and classified as A1 (Table 1), observed at small magnification (20x), in the proximity of the portal space as well as within the parenchyma. Conversely, MCC950/LPs treatment has induced a substantial reduction of inflammatory cells at portal space, with a classification index between A0<A1 (Table 1). Finally, an inflammation index equal to A0 (Table 1) has been achieved in the liver of mice treated with anti-FZD1/MCC950/LPs, even in the presence of steatosis. These results indicate that the anti-FZD1 antibody decoration of the MCC950 loaded LPs improves drug effectiveness, further reducing liver inflammation *in vivo* experimental models.

In Figure 10 B, the images of fibrosis, developed during the treatments, are reported. While CTR and free MCC950 groups have shown high grade of fibrosis (F2), evidenced by the presence of reticulin fibers, groups treated with LP-based formulations, conjugated or unconjugated with anti-FZD1 antibody, have exhibited a strong reduction of the fibrosis (F0<F1, Table 1).

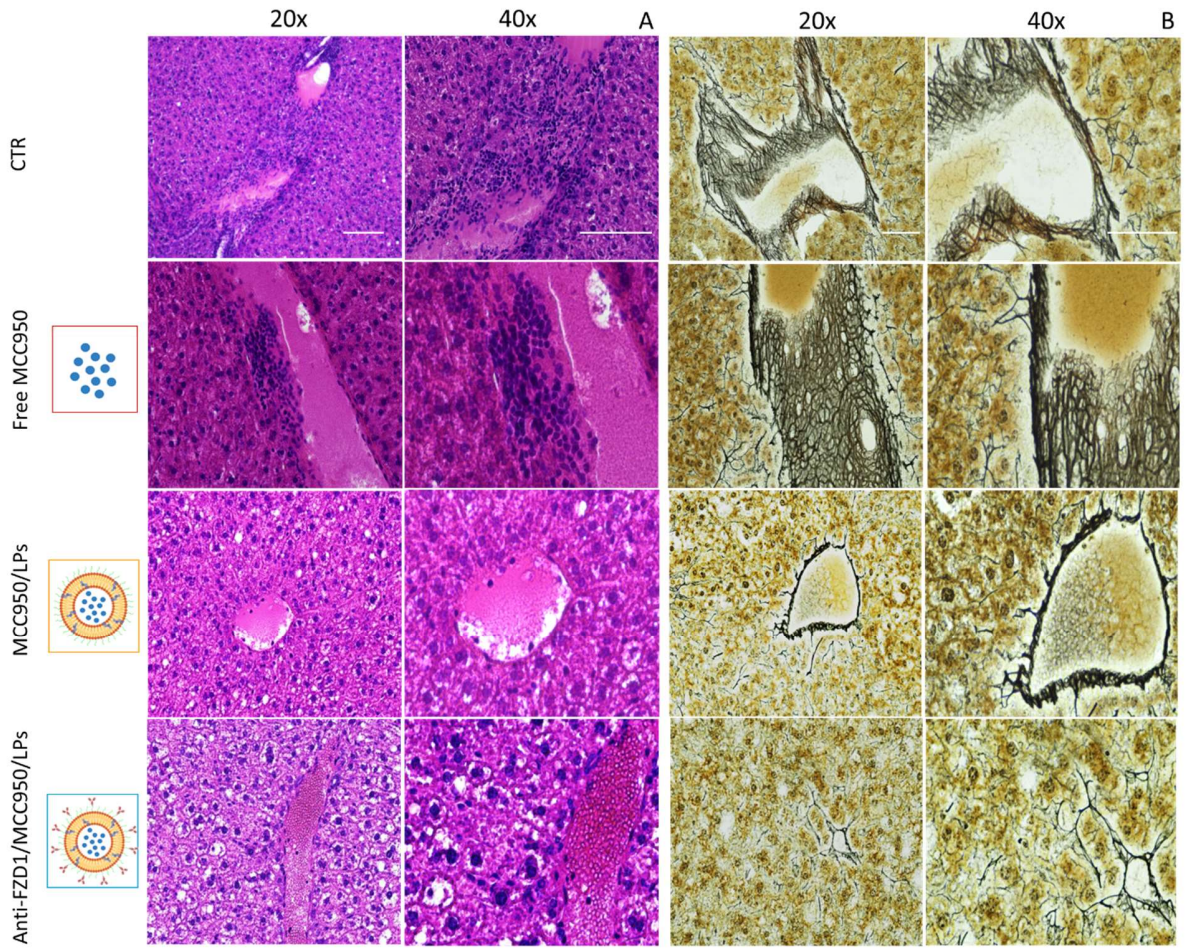

Figure 10. Representative liver sections of high fat diet treated-wild type mice upon administration of the free MCC950, MCC950/LPs and anti-FZD1/MCC950/LPs, stained for He-E (A) and Gomori's reticulin staining (B) at 20x and 40x of magnification. Control group: wild type mice receiving only the high fat diet (CTR).

Table 6. Histological grade of inflammation and fibrosis in liver mice samples treated with free MCC950, MCC950/LPs and anti-FZD1/MCC950/LPs. Control group: wild type mice receiving only the high fat diet (CTR).

Sample	Inflammation grade	Fibrosis grade
CTR	A2	F2
MCC950	A1	F2
MCC950/LPs	A1	F1
Anti-FZD1/MCC950/LPs	A0	F0

DISCUSSION

NASH is a common cause of liver degeneration mediated by inflammation.[21] In particular, the innate immune system represents the first line of defence against the damage-associated molecular patterns produced by host cells.[22] One of the major features exerted by the innate immune cells, is represented by the inflammasome machinery, defined as an "intracellular sensor", also called pattern recognition receptors (PRRs), that, upon danger recognition, assemblies into micrometer-size platform, to promote the release of pro-inflammatory cytokine, such as IL-1β and IL-18, concomitantly with a form of cell death called pyroptosis.[23] So far, five members of the PRR family have been demonstrated involved in the formation of the inflammasome in gastro-intestinal tract: the nucleotide-binding oligomerization domain (NOD) like receptor (NLR) family Pyrin domain containing 1 (NLRP1), NLRP3, NLRP6 and NLR family CARD domain containing 4 (NLRC4).[24-29] The activation of NLRP3 inflammasome, the most characterized inflammasome, has been linked to several IL-1β and IL-18 mediated diseases, thus becoming a potential novel therapeutic target able to delay or prevent disease progression. There are different inflammasome pathway activation systems, as different are the causes of inflammation; however the direct inhibition of NLRP3 by using specific and selective inhibitors leads to the direct resolution of pathological conditions triggered by exogenous causes, as virus, bacteria or fungi induced infections,[30-32] but also endogenous pathological conditions such as atherosclerosis,[33] Alzheimer,[34] and hepatic degeneration from NAFLD.[35] Currently an important challenge is to succeed in conveying and directing drugs able to directly have an effect on the NLRP3. In fact, several studies report on the use of nanovectors that act on molecules that activate inflammasome but are not selective towards the NLRP3. In this perspective, an ideal candidate for NLRP3 inflammasome inhibition is the

MCC950, a recently discovered small molecule,[36] that is highly specific for NLRP3, and that in liver tissue, has been shown to reduce immune cells infiltration and to mitigate liver injury and progression toward a fibrotic status.[37] As reported in several pharmacokinetics studies, MCC950, administered as free drug, is characterized by a very short half-life (3.27 hours), that hampers its use.[36] So far, for the MCC950, administered as free drug, the concentration range explored in *in vitro* studies spans from 10 nM to 10 μM,[38] while it has been intraperitoneal administrated in the range between 10 and 50 mg/Kg in *in-vivo* models.[39, 40] The present study aims to demonstrate that the MCC950, encapsulated into PEGylated LPs, decorated with an antibody targeting inflammasome activated THP-1 cells plasma membrane receptor protein FZD1, inhibits NLRP3 activation using concentrations that are 10-times lower than the lowest drug concentration tested in *in-vitro* and *in-vivo* studies in respect to the free administrated MCC950. This achievement suggests that the proposed formulations can dampen down neutralization (half-life) and dispersion rate of the drug, that normally takes place in the bloodstream. The FZD1 targeted and non-targeted LPs are characterized by hydrodynamic diameters lower than 200 nm for both the nanoformulations, with ζ-potential values that indicate high colloidal stability in aqueous media. The improved ability of targeted LPs, with respect to the not targeted ones, to be cell internalized has been proved by using luminescent CDs containing optically traceable formulations for the *in vitro* uptake study performed by confocal microscopy. In particular, inflammasome activated THP-1 cells became fluorescent positive after 4-8 hours post treatment with antibody-decorated LPs containing MCC950, whereas untargeted LPs are still present externally to the cytoplasmic membrane after 8 hours, hence confirming the expression of FZD1 onto those cells[41] and a faster drug uptake in the case of the targeted LPs. Moreover, the experiments have confirmed the previously reported[42] non-toxic effect, in terms of cell viability, of MCC950, under the explored

experimental conditions, either as free or fully encapsulated formulations, when tested in human monocyte THP-1, tumorigenic and normal liver cell lines, HLF and HEPA-RG, respectively. The activation and inhibition of the NLRP3 inflammasome has been investigated by looking for the presence/absence of ASC perinuclear *puncta* in THP-1 cells, by immunofluorescence. Using free 1 nM MCC950, an activation rate of inflammasome similar that found for either empty LPs and positive control (LPS/nigericin) has been detected. Conversely, for cells treated with the complete formulations (anti-FZD1/MCC950/LPs 1 nM), no activation of inflammasome has been observed. The results pinpoint that the novel strategy, to reformulate the MCC950, based on PEG stabilized LPs, is able to significantly curtail the threshold of MCC950 doses, still maintaining the same therapeutic efficacy of the drug free administration. These original designed LP-based systems, featuring the relevant advantage of using lower working concentration for the same therapeutic efficiency of a free administration, opens promising therapeutic perspectives for MCC950 in the treatment of inflammatory-driven diseases. Two independent studies have reported that IL-1 family cytokines are determinant keystones in the evolution of fibrosis and cirrhosis, which is the 12th leading cause of death in the United States.[19, 43] Our in vivo data, obtained by using wild type mice fed with high fat diet and DSS to induce the liver inflammation, as reported in literature,[44] show that, upon treatment with complete nanoformulations (anti-FZD1/MCC950/LPs), inflammatory foci formation in liver parenchyma can prevent inflammatory foci formation in liver parenchyma and a reduction of fibrosis can be achieved, compared to control and empty LPs treated mice. Moreover, it has been reported in literature a significant reduction of fibrosis and steatohepatitis through the abrogation of inflammation when free-administered MCC950 was used at 10-50 mg/kg.[39, 45] With our PEG-LPs we confirm these results, but using a significantly lower amount of MCC950, without observing any on steatosis or cholesterol crystal deposition.

CONCLUSIONS

Here, we have demonstrated that LPs encapsulating MCC950 and decorated with a specific antibody against FZD1 receptor, reduces hepatic inflammatory infiltration and modulates fibrotic progression of steatosis in *in vivo* model. *In vitro* studies have proven the efficacy of the anti-FZD1/MCC950/LPs (1 nM) to dampen down the inflammasome activation in THP-1 cells, IL-1β release and fibrosis fibers formation such as reticulin fibers. The lower concentration of MCC950 necessary to observe these phenotypes, when loaded in the LPs, makes the application of our nanoformulations a promising pharmacological tool for development of therapy able to revert inflammatory- and fibrosis-driven NAFLD.

EXPERIMENTAL SECTION

1. Preparation of LPs-based formulations

Empty LPs were prepared by exploiting the reverse phase evaporation method and following the experimental procedure reported in M.P. Scavo et al.[6] with some modifications. Briefly, 274 µL of lipid mix chloroform solution (56.09 mg/mL, liposome Kit L-α-phosphatidylcholine:stearylamine: cholesterol, 7:3:1 molar ratio), Sigma Aldrich) and 13.5 µL of a chloroform solution of DSPE-PEG (0.1 µg/µL, Avanti Polar Lipids) were mixed in 2.738 mL of ether/chloroform (1:1, v/v) solution. After stirring and subsequent addition of ultrapure water (3 mL) into the organic lipid solution, consecutive cycles consisting of sonication and cooling down on ice were performed within 10 minutes. The mixture was then stirred for 16 hours at 25°C to allow the complete evaporation of the organic phase. Finally, LPs were extruded by using a manual mini-extruder (Avanti Polar Lipids) equipped with 200 nm and 100 nm filters.

LPs loaded with MCC950 (MCC950/LPs) were prepared using 3 mL of aqueous MCC950 (Sigma Aldrich) solutions at different concentrations (0.3, 0.5 and 1 mg/mL) instead of pure water.

After synthesis of luminescent CDs according to the experimental procedure reported in A. Panniello et al.,[18] LPs co-loaded with MCC950 and CDs (MCC950-CD/LPs) were prepared by introducing 3 mL of a MCC950 aqueous solution (1 mg/mL) and 5 mg of CDs dispersion in chloroform (620 mg/mL) in the organic phase. For all the preparations, after extrusion, excess of lipids, non-embedded drug and/or CDs were removed by three centrifugation cycles at 18°C (Centricon centrifugal filter). For the preparation of LPs conjugated with FZD1 antibody (anti-FZD1/MCC950/LPs and anti-FZD1/MCC950-CD/LPs), LPs were previously surface-functionalized with carboxylic groups (LPs-COOH). For this purpose, DSPE-PEG2000-COOH (Avanti Polar Lipids) was used instead of DSPE-PEG2000.

After the LPs purification, 1650 µL of LPs-COOH dispersion in ultrapure distilled water were activated by using phosphate buffer solution (PBS) of sulfo-NHS (250 µL 0.1 M) and EDC (10 µL 1M). After gentle stirring for 15 minutes at room temperature, the activated LPs-COOH were incubated with anti-FZD1 antibody (ABCAM, Cambridge, UK, 10 µg) and the mixture was left to gently stir for 1.5 hours at 28 °C. Finally, the nanoformulations were purified by three centrifugation cycles at 18 °C (Centricon centrifugal filter) to remove unbound antibody and re-dispersed in PBS (10 mM, pH 7.5). For all the obtained formulations, evaluation of their concentration expressed as mg/mL has been carried out by freeze-drying of aqueous samples.

2. Characterization of the LPs-based formulations in terms of size, morphology, colloidal stability and optical properties

Hydrodynamic diameter, size distribution and colloidal stability of the different LPs samples were evaluated by using a Zetasizer Nano ZS, Malvern Instruments Ltd., Worcestershire, UK

(DTS 5.00), (samples dilution 1:100 in ultrafiltrated water). All reported data are presented as mean values ± standard deviation (three replicates).

TEM investigation was performed by means of a Jeol JEM-1011 microscope, working at an accelerating voltage of 100 kV, and TEM images were acquired by an Olympus Quemesa Camera (11 Mpx). The samples were prepared by dropping a LPs aqueous suspension on the 400 mesh amorphous carbon-coated Cu grid and letting the solvent to evaporate.

UV-Vis absorption measurements were performed by means with a VARIAN CARY® 5000 UV-Vis-NIR double beam spectrophotometer.

Attenuated total reflection Fourier-Transform Infrared (ATR-FT IR) spectra of samples were recorded by means of a PerkinElmer Spectrum One Fourier Transform Infrared spectrometer equipped with a 4 mm diameter diamond microprism as internal reflection element. All the spectra were recorded in the range of 400-4000 cm-1 with a resolution of 4 cm^{-1} (16 scans).

The steady-state PL emission spectra were recorded by using a Fluorolog 3 spectrofluorometer (HORIBA Jobin-Yvon) equipped with a 450 W Xe lamp as excitation light source, coupled with a double-grating excitation and emission monochromators.

TR-PL measurements were performed by time correlated single photon counting (TSTPC) technique, with a FluoroHub (HORIBA Jobin-Yvon). The samples were excited at 375 nm by a picosecond laser diode (NanoLED 375L). The PL signals were detected by a picosecond photon counter (TBX ps Photon Detection Module, HORIBA Jobin-Yvon). The time resolution of the experimental setup was set to ≈ 200 ps. The decay function has been determined from the output histogram performing a fitting procedure using a multi-exponential model by means of the DAS Analysis® software that allowed us to derive the average lifetime (τavg). The goodness of the fit

was controlled by making use of a residual plot and by the $\chi 2$ parameter (as usually accepted, only fitted curves with $\chi 2 < 1.2$ were considered).

Finally, the absolute PL quantum yield (PLQY) measurements were also performed on the CD and CD/LPs samples by means of a "Quanta-phi" integration sphere coated with Spectralon® mounted in the optical path of the spectrofluorometer.

3. Evaluation of encapsulation efficiency and drug loading of MCC950

The encapsulation efficiency percentage (EE%) of the drug encapsulated in LPs and drug loading percentage (DL%) were evaluated by recording UV-Vis absorbance spectra of LPs samples. An aqueous solution containing empty LPs at the same concentration of MCC950 loaded LPs in terms of lipids was used as baseline. EE% was calculated according to the following formula: EE% = (Wt/Wi)*100, where Wt is the total amount of MCC950 in the nanoformulations and Wi is the total starting quantity of drug introduced for the preparation. DL% was calculated as follows: DL % = (W_t/W_{LPs})*100 where WLPs represents the weight of LPs. A calibration curve of MCC950 was obtained by recording the absorbance at 283 nm of standard aqueous solutions of MCC950 at concentrations ranging from 0.025 to 0.3 mg/mL.

4. Cell Culture

2D HEPA-RG cells were cultured using HBM medium (GibCo), a specific medium for this cell line, added with 10% of fetal bovine serum, 1% of penicillin/streptomycin and 1% of glutamine. While, THP-1 and HLF were cultured in DMEM from GibCo, which was added with 10% of fetal bovine serum, 1% of penicillin/streptomycin and 1% of glutamine. When the cell line reached 70% of confluence, the cell layer was rinsed with PBS, and trypsinized, for *in-vitro* experiments. For the co-cultures, the THP-1 cells were sown into the Falcon® cell culture inserts (VWR, Darmstadt, Germany) for the co-cultivation using DMEM from GibCo, which was added with 10% of fetal

bovine serum, 1% of penicillin/streptomycin and 1% of glutamine, at a density of 0.65 × 105 cells for each insert; while the HEPA-RG or HLF cells, were directly sown and cultured with the usual medium, at density of 1.3×10^5 cells per cm^2. After 24 hours of co-culture procedures, the THP-1 cells were treated with LPS/nigericin for 4 hours, for inflammasome priming and activation, respectively. After 4 hours, they were treated with the different LPs samples. The LPs formulations were administrated also directly to the hepatic cell lines at the same concentration to determine the cytotoxicity.

5. Uptake study on LPs-based formulations

The LPs uptake experiments were carried out as described in the modified experimental protocols reported by Scavo et al..[6] Briefly, THP-1 cells (100,000 cells/well) were seeded in a 6-well plate for uptake studies and when they reached 70% of confluence, luminescent MCC950-CD/LPs and AntiFZD1/MCC950-CD/LPs were added to THP-1 cell line at concentration of 0.0336 mg/mL and 1 nM for CDs and MCC950 respectively. The LPs based formulations were added to fresh medium in each well, and the uptake was monitored at fixed time points, namely at 1, 4 and 8 hours (T0, T2, T3), using the Eclipse Ti2 by Nikon confocal microscope (Nikon, Tokyo, Japan). The images were acquired by using a Kr-Ar and Ar lasers for the observation of the luminescent LPs (555 nm) or bright field for the visualization of the cells (40× magnification).

6. Cells Proliferation Assay

In the cell proliferation assay a modified protocol reported by Depalo et al.,[11] and the Cell-Titer 96® AQueous One Solution Cell Proliferation Assay, Promega were used to determine viability in all tested cell lines. Briefly, THP-1, HEPA-RG and HLF cell lines were seeded into 96-well plates at a density of 2×10^3 cells/well. After 24 hours, the cells were treated with free drug (MCC950), MCC950/LPs and antiFZD1/MCC950/LPs at 1 nM of concentrations for 24, 48 or 72

hours. For the treatment with empty LPs, the cells were incubated with the same lipid concentration used in testing drug loaded LPs. Untreated cells were used as control. After cell incubation with the different samples, cells were treated with the MTS tetrazolium compound for three additional hours and the absorbance was measured at a wavelength of 490 nm using a Perkin Elmer Victor Plate Reader (Mechelen, Belgium).

7. In vitro activation of the NLRP3 inflammasome, *punctum* formation and its inhibition

The NLRP3 inflammasome activation was carried out in two subsequential steps. Cells were firstly primed with lipopolysaccharide (LPS, Sigma-Adrich, 1 μg/mL) for 4 hours, followed by the activation step with Nigericin (6 μM) for 30 minutes. For the NLRP3 inflammasome inhibition, cells were incubated, alongside the LPS, with MCC950, at final concentration of 1 nM, and the same concentration of drug was used when it was incapsulated into the different LPs samples for 4 hours before the addition of Nigericin. Before the priming step, THP-1 monocytes were in M0 state, however, upon treatment with 1 ug/mL of LPS for 4 hours, cell underwent toward a phenotypic switch characterized by a M1 polarization state, the pro-inflammatory phenotype, with increased inflammasome related genes (such as pro-IL-1b). In the case of empty LPs, the cells were incubated with the same lipid concentration used in testing drug loaded LPs. After 30 minutes, THP-1 cells were fixed with 96° cold ethanol for 30 minutes at -20°C. Untreated cells were used as control. The cells were observed for the inflammasome activation or inhibition by monitoring the presence of apoptosis-associated speck-like protein containing a CARD (ASC) *punctum* using immunofluorescence. Briefly, after the fixation step, cells were washed 3 times in phosphate buffer (PBS), permeabilized with 0.5% TRITON-X100 (Sigma-Aldrich) in PBS for 10 minutes and the non-specific sites were blocked using the 5% BSA (Bovine Serum Albumin, Sigma-Aldrich) in PBS for 1 hour at room temperature. Then, the antibody for ASC was added

(rabbit polyclonal 1:400 Cell signaling) and incubated for 16 hours. Treated cells were incubated with a specific red fluorescent conjugated secondary IgG Alexa 555(Invitrogen) ($\lambda_{abs,max}$ 555 nm) for 1 hour and mounted using Prolong Gold Antifade reagent containing DAPI ($\lambda_{abs,max}$ 345 nm). Images were acquired with a Nikon Eclipse Ti2 fluorescence microscope. The images were acquired by exciting with Kr-Ar and Ar lasers fitted with 555 and 358 nm band-pass filters, respectively, for the ASC red channel (555 nm) and for the DAPI blue channel (358 nm) at ×40 magnification and the number of present puncta was determinated using the Nikon Eclipse Ti2 (NIS) software. Briefly, five fields were acquired for each condition and the percentage of the nuclei presenting the puncta was calculated from the total of the nuclei present. The fluorescence intensity was quantified by using an exposure time of 500 ms per acquisition for all the investigated samples.

8. IL-1β ELISA assay

The conditioned medium, derived from the co-culture of THP-1-HEPA-RG or THP-1-HLF cells, were analyzed for IL-1β, and an ELISA kit (abCam, Cambridge, UK) was used, according to the protocol indicated by the manufacturer. The optical density (O. D.) was read at 450 nm within 10 min after adding the stop solution by using a Bio-RAD spectrophotometer.

9. Mice treatments

A pilot *in vivo* study was carried out by using twelve 9-week-old male wild type mice (C57BL/6J), obtained from Charles River (Calco, Italy). Upon arrival, all mice were kept in temperature, air, and light-controlled conditions (light on from 7 AM to 7 PM) and received water ad libitum and a high fat diet throughout the duration of the trial (30 days). Furthermore, all animals received also Dextran-Sulphate-Sodium(DSS) (1% in the drinking water) and adminstrated in cycles, each cycle consisting of 7 days of DSS administration followed by a 7-day interval with

normal drinking water, for 30 days, to induce the liver inflammation.[19, 20] All animals received human care according to the criteria outlined in the Guide for the Care and Use of Laboratory Animals. The mice were divided into four groups (three for each group) to undergo different treatments: the first group was used as a control group by receiving only the high fat diet, the second one received the intraperitoneal injection of the free MCC950, the third one received MCC950/LPs (1 mg/Kg), and the last one received the AntiFZD1/MCC950-CD/LPs. The tested drug concentration was 1 mg/Kg for all administrated samples. The duration of all treatments was 30 days during which the administrations were carried out 2 times per week. After one week from the last treatment, the animals were sacrificed and the livers were analysed by pathology investigation.

10. Mice liver evaluation

The whole liver was sampled according to the serial-step, whole-specimen sectioning technique previously described by M. Barone et al..[40] Briefly, the liver was fixed in 10% neutral buffered formalin for 12–24 hours and embedded in paraffin. Then, 4 μ-thick consecutive slides were prepared for histological, immunohistochemical, immunofluorescence, and in situ hybridization studies. The presence of inflammatory foci was confirmed by microscopic observation of consecutive sections using haematoxylin–eosin (He-E) and Gomori's reticulin staining (GS).

11. Statistical analysis

A statistical analysis was performed with Sigma-Stat 3.1 software, using one-way analysis of variance (ANOVA). The differences noticed were statistically significant at $p < 0.005$ or $p < 0.001$. When mean equality among groups was rejected by the one-way ANOVA, the Bonferroni method was applied for the comparison.

ASSOCIATED CONTENT

Supporting Information

ATR FT-IR spectroscopic characterization of LPs-based formulations; Optical and morphological characterization of the *"as synthesized"* CDs; Quantitative evaluation of encapsulation efficiency of CDs; Characterization of the LPs-based formulations conjugated with the anti-FZD1 antibody; Quantitative evaluation of the FZD1 antibody amount conjugated onto surface of the LPs-based formulations (PDF).

Author Contributions

Conceptualization: Roberto Negro, Rita Mastrogiacomo, Maria Principia Scavo Nicoletta Depalo; Methodology: Livianna Carrieri, Federica Rizzi, Valentina Arrè, Elisabetta Fanizza, Annamaria Panniello, Giusy Bianco, Nicoletta Depalo, Maria Principia Scavo; Validation: Maria Principia Scavo, Nicoletta Depalo, Elisabetta Fanizza, Annamaria Panniello, Marinella Striccoli, Maria Lucia Curri, Gianluigi Giannelli; Formal Analysis: Elisabetta Fanizza, Maria Principia Scavo, Nicoletta Depalo, Livianna Carrieri, Federica Rizzi, Valentina Arrè, Roberto Negro, Rita Mastrogiacomo, Gianluca Minervini,; Investigation, Livianna Carrieri, Federica Rizzi, Valentina Arrè, Roberto Negro, Rita Mastrogiacomo, Gianluca Minervini, Raffaele Armentano, Giusy Bianco, Roberto Comparelli; Resources: Maria Lucia Curri, Gianluigi Giannelli, Roberto Comparelli, Raffaele Armentano, Marinella Striccoli; Data Curation: Maria Principia Scavo, Nicoletta Depalo, Rita Mastrogiacomo, Federica Rizzi; Writing—original draft preparation, Rita mastrogiacomo, Roberto Negro, Livianna Carrieri, Maria Principia Scavo, Nicoletta Depalo; Writing—review and editing, Maria Principia Scavo, Nicoletta Depalo, Federica Rizzi, Rita Mastrogiacomo, Maria Lucia Curri; Supervision Maria Lucia Curri, Gianluigi Giannelli; project administration: Maria Lucia Curri, Gianluigi Giannelli, Maria Principia Scavo, Nicoletta Depalo; funding acquisition: Maria Lucia Curri, Gianluigi Giannelli, Roberto Comparelli, Marinella Striccoli, Nicoletta Depalo.

All authors have read and agreed to the published version of the manuscript.

ACKNOWLEDGMENTS

We acknowledge the Italian Health Ministry for Ricerca Corrente project 2021-2024 "Biomimetic nanoparticles as a new strategy for the transport of drugs in oncological therapies of the gastro-enteric tract", the project PON TITAN "Nanotechnology for cancer immunotherapy", 2021–2023 ARS01_00906 and bilateral project CNR-RFBR (Russia) "Mesoporous silica nanocarriers incorporating plasmonic $Cu_{(2-x)}S$ nanocrystals, fluorophores and 5-fluorouracil and functionalized

with FZD10 antibody for the targeted photo-induced therapy of colorectal cancer" joint research projects in the triennium 2021-2023

ABBREVIATIONS

Non-alcoholic fatty liver disease (NAFLD); polyethylene glycol (PEG)-liposomes (LPs); Frizzled 1 (FZD1); Non alcoholic liver disease (NASH); Transforming growth factor (TGF);hepatocellular carcinoma (HCC); NLR Family Pyrin Domain Containing 3 (NLRP3); interleukin (IL); nanoparticles (NPs); Carbon dots (CDs); LPs encapsulating MCC950 (MCC950/LPs); Encapsulation Efficiency percentage (EE%); Drug Loading percentage (DL%); CDs loaded LPs (CD/LPs); LPs co-loaded with CDs and MCC950 (MCC950-CD/LPs); LPs conjugated with the antiFZD1 antibody (anti-FZD1/MCC950/LPs)(anti-FZD1/MCC950-CD/LPs); pattern recognition receptors (PRRs); nucleotide-binding oligomerization domain (NOD); Nod Like Receptor (NLR); Family Pyrin domain containing 1 (NLRP1); NLR family CARD domain containing 4 (NLRC4)

REFERENCES

1. Huang, Y.; Ge, W.; Zhou, J.; Gao, B.; Qian, X.; Wang, W., The Role of Tumor Associated Macrophages in Hepatocellular Carcinoma. *J Cancer* **2021,** *12*, 1284-1294.
2. Rajapaksha, I., Liver Fibrosis, Liver Cancer, and Advances in Therapeutic Approaches. *Livers* **2022,** *2*, 372-386.
3. Neumann, J.; Schaale, K.; Farhat, K.; Endermann, T.; Ulmer, A. J.; Ehlers, S.; Reiling, N., Frizzled1 Is a Marker of Inflammatory Macrophages, and Its Ligand Wnt3a Is Involved in Reprogramming Mycobacterium Tuberculosis-Infected Macrophages. *The FASEB Journal* **2010,** *24*, 4599-4612.
4. Latz, E.; Xiao, T. S.; Stutz, A., Activation and Regulation of the Inflammasomes. *Nature Reviews Immunology* **2013,** *13*, 397-411.
5. Perera, A. P.; Fernando, R.; Shinde, T.; Gundamaraju, R.; Southam, B.; Sohal, S. S.; Robertson, A. A. B.; Schroder, K.; Kunde, D.; Eri, R., Mcc950, a Specific Small Molecule Inhibitor of Nlrp3 Inflammasome Attenuates Colonic Inflammation in Spontaneous Colitis Mice. *Scientific Reports* **2018,** *8*, 8618.
6. Scavo, M. P.; Cutrignelli, A.; Depalo, N.; Fanizza, E.; Laquintana, V.; Gasparini, G.; Giannelli, G.; Denora, N., Effectiveness of a Controlled 5-Fu Delivery Based on Fzd10 Antibody-Conjugated Liposomes in Colorectal Cancer in Vitro Models. *Pharmaceutics* **2020,** *12*, 650.
7. Zhan, C.; Lin, G.; Huang, Y.; Wang, Z.; Zeng, F.; Wu, S., A Dopamine-Precursor-Based Nanoprodrug for in-Situ Drug Release and Treatment of Acute Liver Failure by Inhibiting Nlrp3 Inflammasome and Facilitating Liver Regeneration. *Biomaterials* **2021,** *268*, 120573.

8. Zhao, Y.; Yang, Y.; Zhang, J.; Wang, R.; Cheng, B.; Kalambhe, D.; Wang, Y.; Gu, Z.; Chen, D.; Wang, B.; Huang, Y., Lactoferrin-Mediated Macrophage Targeting Delivery and Patchouli Alcohol-Based Therapeutic Strategy for Inflammatory Bowel Diseases. *Acta Pharmaceutica Sinica B* **2020,** *10*, 1966-1976.
9. Sun, L.; Ouyang, J.; Zeng, F.; Wu, S., An Aiegen-Based Oral-Administration Nanosystem for Detection and Therapy of Ulcerative Colitis Via 3d-Msot/Nir-Ii Fluorescent Imaging and Inhibiting Nlrp3 Inflammasome. *Biomaterials* **2022,** *283*, 121468.
10. Ma, Q.; Fan, Q.; Han, X.; Dong, Z.; Xu, J.; Bai, J.; Tao, W.; Sun, D.; Wang, C., Platelet-Derived Extracellular Vesicles to Target Plaque Inflammation for Effective Anti-Atherosclerotic Therapy. *Journal of Controlled Release* **2021,** *329*, 445-453.
11. Depalo, N.; Fanizza, E.; Vischio, F.; Denora, N.; Laquintana, V.; Cutrignelli, A.; Striccoli, M.; Giannelli, G.; Agostiano, A.; Curri, M. L.; Scavo, M. P., Imaging Modification of Colon Carcinoma Cells Exposed to Lipid Based Nanovectors for Drug Delivery: A Scanning Electron Microscopy Investigation. *RSC Advances* **2019,** *9*, 21810-21825.
12. Ren, W.; Chen, S.; Liao, Y.; Li, S.; Ge, J.; Tao, F.; Huo, Q.; Zhang, Y.; Zhao, Z., Near-Infrared Fluorescent Carbon Dots Encapsulated Liposomes as Multifunctional Nano-Carrier and Tracer of the Anticancer Agent Cinobufagin in Vivo and in Vitro. *Colloids and Surfaces B: Biointerfaces* **2019,** *174*, 384-392.
13. Karimi, M.; Ghasemi, A.; Sahandi Zangabad, P.; Rahighi, R.; Moosavi Basri, S. M.; Mirshekari, H.; Amiri, M.; Shafaei Pishabad, Z.; Aslani, A.; Bozorgomid, M.; Ghosh, D.; Beyzavi, A.; Vaseghi, A.; Aref, A. R.; Haghani, L.; Bahrami, S.; Hamblin, M. R., Smart Micro/Nanoparticles in Stimulus-Responsive Drug/Gene Delivery Systems. *Chemical Society Reviews* **2016,** *45*, 1457-1501.
14. Nakhaei, P.; Margiana, R.; Bokov, D. O.; Abdelbasset, W. K.; Jadidi Kouhbanani, M. A.; Varma, R. S.; Marofi, F.; Jarahian, M.; Beheshtkhoo, N., Liposomes: Structure, Biomedical Applications, and Stability Parameters with Emphasis on Cholesterol. *Frontiers in Bioengineering and Biotechnology* **2021,** *9*.
15. Arduino, I.; Depalo, N.; Re, F.; Dal Magro, R.; Panniello, A.; Margiotta, N.; Fanizza, E.; Lopalco, A.; Laquintana, V.; Cutrignelli, A.; Lopedota, A. A.; Franco, M.; Denora, N., Pegylated Solid Lipid Nanoparticles for Brain Delivery of Lipophilic Kiteplatin Pt(Iv) Prodrugs: An in Vitro Study. *International Journal of Pharmaceutics* **2020,** *583*, 119351.
16. Latronico, T.; Rizzi, F.; Panniello, A.; Laquintana, V.; Arduino, I.; Denora, N.; Fanizza, E.; Milella, S.; Mastroianni, C. M.; Striccoli, M.; Curri, M. L.; Liuzzi, G. M.; Depalo, N., Luminescent Plga Nanoparticles for Delivery of Darunavir to the Brain and Inhibition of Matrix Metalloproteinase-9, a Relevant Therapeutic Target of Hiv-Associated Neurological Disorders. *ACS Chemical Neuroscience* **2021,** *12*, 4286-4301.
17. Chung, Y. J.; Kim, J.; Park, C. B., Photonic Carbon Dots as an Emerging Nanoagent for Biomedical and Healthcare Applications. *ACS Nano* **2020,** *14*, 6470-6497.
18. Panniello, A.; Di Mauro, A. E.; Fanizza, E.; Depalo, N.; Agostiano, A.; Curri, M. L.; Striccoli, M., Luminescent Oil-Soluble Carbon Dots toward White Light Emission: A Spectroscopic Study. *The Journal of Physical Chemistry C* **2018,** *122*, 839-849.
19. Gäbele, E.; Dostert, K.; Hofmann, C.; Wiest, R.; Schölmerich, J.; Hellerbrand, C.; Obermeier, F., Dss Induced Colitis Increases Portal Lps Levels and Enhances Hepatic Inflammation and Fibrogenesis in Experimental Nash. *Journal of Hepatology* **2011,** *55*, 1391-1399.

20. Shen, B.; Wang, J.; Guo, Y.; Gu, T.; Shen, Z.; Zhou, C.; Li, B.; Xu, X.; Li, F.; Zhang, Q.; Cai, X.; Dong, H.; Lu, L., Dextran Sulfate Sodium Salt-Induced Colitis Aggravates Gut Microbiota Dysbiosis and Liver Injury in Mice with Non-Alcoholic Steatohepatitis. *Frontiers in Microbiology* **2021,** *12*.
21. Bishayee, A., The Inflammation and Liver Cancer. In *Inflammation and Cancer*, Aggarwal, B. B.; Sung, B.; Gupta, S. C., Eds. Springer Basel: Basel, 2014; pp 401-435.
22. Geier, A.; Tiniakos, D.; Denk, H.; Trauner, M., From the Origin of Nash to the Future of Metabolic Fatty Liver Disease. *Gut* **2021,** *70*, 1570.
23. Faria, S. S.; Costantini, S.; de Lima, V. C. C.; de Andrade, V. P.; Rialland, M.; Cedric, R.; Budillon, A.; Magalhães, K. G., Nlrp3 Inflammasome-Mediated Cytokine Production and Pyroptosis Cell Death in Breast Cancer. *Journal of Biomedical Science* **2021,** *28*, 26.
24. Kelley, N.; Jeltema, D.; Duan, Y.; He, Y., The Nlrp3 Inflammasome: An Overview of Mechanisms of Activation and Regulation. *International journal of molecular sciences* **2019,** *20*, 3328.
25. Strowig, T.; Henao-Mejia, J.; Elinav, E.; Flavell, R., Inflammasomes in Health and Disease. *Nature* **2012,** *481*, 278-286.
26. Zhen, Y.; Zhang, H., Nlrp3 Inflammasome and Inflammatory Bowel Disease. *Frontiers in Immunology* **2019,** *10*.
27. Ranson, N.; Kunde, D.; Eri, R., Regulation and Sensing of Inflammasomes and Their Impact on Intestinal Health. *International journal of molecular sciences* **2017,** *18*, 2379.
28. Pirzada, R. H.; Javaid, N.; Choi, S., The Roles of the Nlrp3 Inflammasome in Neurodegenerative and Metabolic Diseases and in Relevant Advanced Therapeutic Interventions. *Genes* **2020,** *11*, 131.
29. Chen, G. Y.; Liu, M.; Wang, F.; Bertin, J.; Núñez, G., A Functional Role for Nlrp6 in Intestinal Inflammation and Tumorigenesis. *The Journal of Immunology* **2011,** *186*, 7187-7194.
30. Sefik, E.; Qu, R.; Junqueira, C.; Kaffe, E.; Mirza, H.; Zhao, J.; Brewer, J. R.; Han, A.; Steach, H. R.; Israelow, B.; Blackburn, H. N.; Velazquez, S. E.; Chen, Y. G.; Halene, S.; Iwasaki, A.; Meffre, E.; Nussenzweig, M.; Lieberman, J.; Wilen, C. B.; Kluger, Y., et al., Inflammasome Activation in Infected Macrophages Drives Covid-19 Pathology. *Nature* **2022,** *606*, 585-593.
31. Dufies, O.; Doye, A.; Courjon, J.; Torre, C.; Michel, G.; Loubatier, C.; Jacquel, A.; Chaintreuil, P.; Majoor, A.; Guinamard, R. R.; Gallerand, A.; Saavedra, P. H. V.; Verhoeyen, E.; Rey, A.; Marchetti, S.; Ruimy, R.; Czerucka, D.; Lamkanfi, M.; Py, B. F.; Munro, P., et al., Escherichia Coli Rho Gtpase-Activating Toxin Cnf1 Mediates Nlrp3 Inflammasome Activation Via P21-Activated Kinases-1/2 During Bacteraemia in Mice. *Nature Microbiology* **2021,** *6*, 401-412.
32. Briard, B.; Malireddi, R. K. S.; Kanneganti, T.-D., Role of Inflammasomes/Pyroptosis and Panoptosis During Fungal Infection. *PLOS Pathogens* **2021,** *17*, e1009358.
33. Fidler, T. P.; Xue, C.; Yalcinkaya, M.; Hardaway, B.; Abramowicz, S.; Xiao, T.; Liu, W.; Thomas, D. G.; Hajebrahimi, M. A.; Pircher, J.; Silvestre-Roig, C.; Kotini, A. G.; Luchsinger, L. L.; Wei, Y.; Westerterp, M.; Snoeck, H.-W.; Papapetrou, E. P.; Schulz, C.; Massberg, S.; Soehnlein, O., et al., The Aim2 Inflammasome Exacerbates Atherosclerosis in Clonal Haematopoiesis. *Nature* **2021,** *592*, 296-301.
34. Zhang, Y.; Dong, Z.; Song, W., Nlrp3 Inflammasome as a Novel Therapeutic Target for Alzheimer's Disease. *Signal Transduction and Targeted Therapy* **2020,** *5*, 37.

35. Thomas, H., A Critical Role for the Nlrp3 Inflammasome in Nash. *Nature Reviews Gastroenterology & Hepatology* **2017,** *14*, 197-197.
36. Coll, R. C.; Robertson, A. A. B.; Chae, J. J.; Higgins, S. C.; Muñoz-Planillo, R.; Inserra, M. C.; Vetter, I.; Dungan, L. S.; Monks, B. G.; Stutz, A.; Croker, D. E.; Butler, M. S.; Haneklaus, M.; Sutton, C. E.; Núñez, G.; Latz, E.; Kastner, D. L.; Mills, K. H. G.; Masters, S. L.; Schroder, K., et al., A Small-Molecule Inhibitor of the Nlrp3 Inflammasome for the Treatment of Inflammatory Diseases. *Nature Medicine* **2015,** *21*, 248-255.
37. Mridha, A. R.; Wree, A.; Robertson, A. A. B.; Yeh, M. M.; Johnson, C. D.; Van Rooyen, D. M.; Haczeyni, F.; Teoh, N. C. H.; Savard, C.; Ioannou, G. N.; Masters, S. L.; Schroder, K.; Cooper, M. A.; Feldstein, A. E.; Farrell, G. C., Nlrp3 Inflammasome Blockade Reduces Liver Inflammation and Fibrosis in Experimental Nash in Mice. *Journal of Hepatology* **2017,** *66*, 1037-1046.
38. Das, B.; Sarkar, C.; Rawat, V. S.; Kalita, D.; Deka, S.; Agnihotri, A., Promise of the Nlrp3 Inflammasome Inhibitors in in Vivo Disease Models. *Molecules* **2021,** *26*, 4996.
39. Jiao, J.; Zhao, G.; Wang, Y.; Ren, P.; Wu, M., Mcc950, a Selective Inhibitor of Nlrp3 Inflammasome, Reduces the Inflammatory Response and Improves Neurological Outcomes in Mice Model of Spinal Cord Injury. *Frontiers in Molecular Biosciences* **2020,** *7*.
40. Barone, M.; Maiorano, E.; Ladisa, R.; Cuomo, R.; Pece, A.; Berloco, P.; Caruso, M. L.; Valentini, A. M.; Iolascon, A.; Francavilla, A.; Di Leo, A.; Ierardi, E., Influence of Ursodeoxycholate-Enriched Diet on Liver Tumor Growth in Hbv Transgenic Mice. *Hepatology* **2003,** *37*, 880-886.
41. Zhang, L.; Jiang, Y.-H.; Fan, C.; Zhang, Q.; Jiang, Y.-H.; Li, Y.; Xue, Y.-T., Mcc950 Attenuates Doxorubicin-Induced Myocardial Injury in Vivo and in Vitro by Inhibiting Nlrp3-Mediated Pyroptosis. *Biomedicine & Pharmacotherapy* **2021,** *143*, 112133.
42. Gluchowski, N. L.; Becuwe, M.; Walther, T. C.; Farese, R. V., Lipid Droplets and Liver Disease: From Basic Biology to Clinical Implications. *Nature Reviews Gastroenterology & Hepatology* **2017,** *14*, 343-355.
43. Barbier, L.; Ferhat, M.; Salamé, E.; Robin, A.; Herbelin, A.; Gombert, J.-M.; Silvain, C.; Barbarin, A., Interleukin-1 Family Cytokines: Keystones in Liver Inflammatory Diseases. *Frontiers in Immunology* **2019,** *10*.
44. Yu, L.; Hong, W.; Lu, S.; Li, Y.; Weng, X.; Feng, Z., Nlrp3 Inflammasome in Non-Alcoholic Fatty Liver Disease and Steatohepatitis: Therapeutic Targets and Treatment. *Frontiers in Pharmacology* **2022**, 682.
45. Yan, W.; Shen, Y.; Huang, J.; Lu, L.; Zhang, Q., Mcc950 Ameliorates Acute Liver Injury through Modulating Macrophage Polarization and Myeloid-Derived Suppressor Cells Function. *Frontiers in Medicine* **2021,** *8*.

Table of Contents Graphic

TOC graphic is entirely original, unpublished artwork

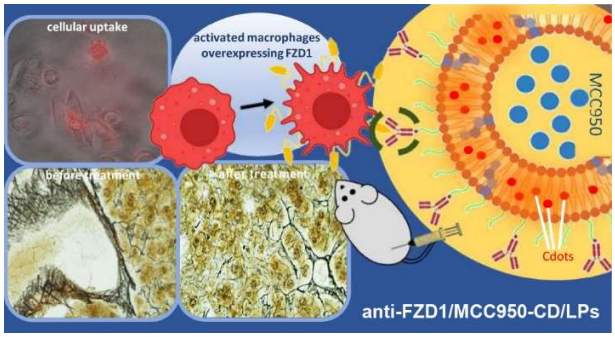
cellular uptake
activated macrophages
overexpressing FZD1
MCC950
before treatment
after treatment
Cdots
anti-FZD1/MCC950-CD/LPs